Acta Cryst. (1990). A46, 271-284

Accurate Structure Analysis with Synchrotron Radiation. The Electron Density in Al_2O_3 and Cu_2O

BY A. KIRFEL

Universität des Saarlandes, FR Kristallographie, D-6600 Saarbrücken 11, Federal Republic of Germany

AND K. EICHHORN

HASYLAB/DESY, Notkestrasse 85, D-2000 Hamburg 52, Federal Republic of Germany

(*Received* 14 *June* 1989; *accepted* 9 *November* 1989)

Abstract

Accurate room-temperature structure analyses have been carried out on the two well known structures of cuprite, Cu_2O, and corundum, α-Al_2O_3, using synchrotron radiation, in order to assess the accuracy of single-crystal X-ray diffraction data that can be obtained with such a source. The two compounds were chosen since results can be rigorously cross checked against deposited data from careful X-ray tube measurements which have been analyzed in terms of electron-density distributions. The synchrotron data were collected on the five-circle diffractometer at HASYLAB in the dedicated mode of DORIS II (3·7 GeV) within normal beam time allowance at the same wavelengths as the tube experiments. The final Cu_2O data set included 21 'forbidden' reflections whose intensities cannot be measured using tube radiation. The intensities of these latter reflections turned out to be predominantly determined by the anisotropic vibration of Cu. Refinements using multipole expansion models yielded agreement indices $R = 0{\cdot}0173$ and 0·0078 for Cu_2O and Al_2O_3, respectively. Structure factors as well as static-model deformation properties including electric-field gradients are compared with the corresponding literature results. Most findings are in satisfactory agreement implying that high-quality diffraction data can be obtained with a synchrotron-radiation source within reasonable time, provided proper attention is given to the experiment and the data-reduction procedure. In particular, the use of synchrotron radiation allows recording of weak and very weak reflection intensities with an accuracy that could never be achieved in conventional tube experiments. An additional data collection on Cu_2O in parasitic mode (5·3 GeV) shows that under less-favorable conditions data can also be collected at a synchrotron-radiation source with an accuracy sufficient for standard structure analyses.

Introduction

Increasingly during the last decade, synchrotron radiation has attracted the attention of crystallographers to make use of its unique properties for a large variety of experiments. Most of these are novel while 'conventional' structure analyses, especially on the level of an analysis of fine structure features, like electron-density distributions and thermal vibrations, are still rare.

In principle, synchrotron radiation offers important advantages for accurate work. Its tunability in energy and in particular its high intensity and small divergence allow the collection of virtually extinction- and absorption-free data on microcrystals (Bachmann, Kohler, Schulz & Weber, 1985). With normal-sized crystals it offers the opportunity of improving the accuracy of weak reflection intensities beyond that achievable with sealed X-ray tubes. Because of the limited access to synchrotron-radiation sources, accuracy and resolution of conventionally collected data sets could be considerably enhanced by combining them with synchrotron measurements of selected reflections.

This principal advantage may, however, be easily offset by the instability of the synchrotron source, both in space and time, and by related experimental and data processing problems.

Thus, not only scarcity of beam time but also lack of experience with the data quality that can be obtained from the available instruments seem to have discouraged accurate structure studies. Encouragement may come from feasibility studies. Nielsen, Lee & Coppens (1986) have carried out such a study at CHESS (Cornell University), collecting data on an organometallic compound of hexagonal symmetry at the short wavelength of 0·302 Å. Their results are a demonstration that high-quality data can be obtained with synchrotron radiation, provided proper precautions are taken.

In order to assess the accuracy that can be obtained on the five-circle diffractometer at HASYLAB/DESY (Kupcik, Wendschuh-Josties, Wolf & Wulf, 1986), we have performed another feasibility study, with a somewhat different approach from that of the above authors. While their results can be judged from their unquestionable internal consistency and the features

0108-7673/90/040271-14$03.00

of the resulting deformation density maps, they have not been compared with tube data. We chose to collect data on the two well known compounds cuprite, Cu_2O, and corundum, α-Al_2O_3, for direct comparison with earlier investigations. Restori & Schwarzenbach (1986) and Lewis, Schwarzenbach & Flack (1982) have studied both compounds thoroughly by means of conventional single-crystal diffractometry. Hereafter these studies are referred to as RS and LSF, respectively. In both cases the data were refined with multipole expansion models to agreement indices close to or even below 0·01 and are therefore generally considered very accurate. Additional reasons for selecting Cu_2O and Al_2O_3 are given below.

The aim of our work was therefore primarily the assessment of an appropriate data collection and reduction strategy and of the data accuracy. The study was conducted in the following steps:

(*a*) measurement of data sets (as complete as possible within the allocated beam time) at the wavelengths of the tube experiments by RS and LSF;

(*b*) data reduction according to the special conditions of synchrotron radiation;

(*c*) comparison of the derived structure factors with the literature data;

(*d*) structure refinements with independent-atom (IAM) and multipole-expansion models: for both compounds synchrotron data and literature data separately, for Cu_2O also combined tube and synchrotron data (see below).

Structures and samples

Crystallographic data for both compounds are summarized in Table 1. The structure of corundum has been described in detail by LSF. Here it suffices to mention that it is composed of AlO_6 octahedra with O tetrahedrally coordinated by Al atoms. Although bonding is usually described as essentially ionic, LSF derived significant deformation density features, with the oxygen charge distribution being polarized towards the adjacent Al atoms.

Corundum is well suited as standard material since the high symmetry allows collection of sufficient numbers of equivalent reflections for the determination of internal consistency and the detection of multiple-scattering effects. It is chemically stable, and the hardness ($H = 9$) of the material and its elastic constants (Landoldt-Börnstein, 1966) imply little TDS. The light elements preclude problems caused by absorption of Ag Kα radiation. Finally, as kindly suggested by D. Schwarzenbach, perfectly spherical Verneuil-grown crystals with negligible Cr contamination and diameters of 0·10–0·25 mm could be obtained from the firm Jean Sandoz et fils, SA (CH-1482 Cugy, Switzerland). The crystal selected for the measurements had a diameter of 0·200 mm.

Table 1. *Crystallographic data*

	Cuprite, Cu_2O Cubic	Corundum, α-Al_2O_3 Hexagonal
a_o (Å)	4·2685 (5)	4·7570 (6)
c_o (Å)		12·9877 (35)
V_c (Å^3)	77·773	254·52
Space group	$Pn\bar{3}m$	$R\bar{3}c$
Z	2	6
Atoms	Cu 4(*b*) (0, 0, 0; $\bar{3}m$)	Al 12*c*(0, 0, *z*; 3)
	O 2(*a*)($\frac{1}{4}, \frac{1}{4}, \frac{1}{4}$; $\bar{4}3m$)	O 18(*e*)(*x*, 0, $\frac{1}{4}$; 2)
M_r	143·09	101·96
D_x (Mg m^{-3})	6·104	3·983
μ(Ag Kα)(mm^{-1})	13·881	0·657
μR	1·20	0·065

The structure of semi- and photoconducting cuprite has attracted much interest by both experimental crystallographers and theoreticians. The outstanding feature is a perfectly linear and symmetric O–Cu–O arrangement (Cu–O 1·848 Å) as a result of the two interpenetrating lattice complexes of Cu and O which are *F* and *I*, respectively. This Cu coordination requires bonding that is not purely ionic. Theoretical calculations by Nagel (1985) and Marksteiner, Blaha & Schwarz (1986) indicated a Cu d^8 plus doubly occupied $3d_{z^2}$–$4s$ hybrid state which allows removal of charge from the bond axis resulting in a Cu–O distance significantly shorter than that permitted by the ionic radii.

From its symmetry, hardness ($H = 4$) and stability at ambient temperatures, cuprite seems also well suited as standard material though absorption and TDS ($\Theta_D = 184$ K) are less favorable than in corundum. As an interesting consequence of the special positions of the atoms the structure factors can be divided into four parity groups with different mean intensities. The contributions of each class characterized by even (*e*) and odd (*o*) Miller indices are:

M(Cu), *M*(O), *M*(Cu)		*Oct*(O),	H_1(Cu), *H*(O) H_1(Cu)	*eee* *ooo*	*s* *s*
	M(O),	*Q*(Cu),	H_2(Cu), *H*(O)	*ooe*	*w*
		Q(Cu), *Oct*(O),	H_2(Cu)	*eeo*	*vw*

(*s* = strong, *w* = weak, *vw* = very weak), *M*, *Q*, *Oct*, $H_{1,2}$ denote atom-centered multipolar density distributions up to hexadecapoles (Kurki-Suonio, 1977), including the U_{12}(Cu) harmonic temperature-factor element into *Q*(Cu) and the free-atom scattering factors into *M*.

This *reflection scheme* shows that the bulk density distribution is determined by the first three parity groups alone. For spherically symmetric probability distribution functions (p.d.f.), all reflections (*eeo*) have zero intensities due to general or special absence rules. Since *M*(Cu) dominates all other contributions, the density fine structure is mainly accessible in the (*ooe*) and (*eeo*) reflections. A thorough structure and electron-density analysis therefore requires accurate measurements of the so-called 'oxygen' (*ooe*) reflections *and* the 'forbidden' (*eeo*) reflections. The latter

especially are expected to be decisive for a separation of anisotropic thermal smearing and chemical bonding effects. They are also important for the calculation of difference density maps, since their omission produces pseudo-symmetric patterns. With tube radiation RS failed to observe more than two 'forbidden' reflections (221, 421), and the reported $I/\sigma(I)$ are hardly significant.

Thus, for cuprite the synchrotron measurements were intended as both an accuracy test and an enhancement of the 100 K data of RS in order to contribute to the understanding of the electron-density distribution.

From a natural sample of imprecisely specified origin (Canada), crystal spheres were prepared in a grinder. The crystal finally selected for the measurements was a sphere of 0·173 mm diameter (maximum asphericity 5 μm).

Experimental

All measurements were carried out on the five-circle diffractometer at HASYLAB beamline D3. In principle, this instrument is a commercial STOE four-circle diffractometer with modified software (Wendschuh-Josties & Wulf, 1989) and angular resolution of 0·001°. A fifth circle permits rotation of the goniostat about the primary-beam axis. For conventional diffraction experiments the scattering plane is always vertical in order to minimize beam divergence and to maximize the intensity yield. A combined intensity/polarization monitor (Smend, Schaupp, Czerwinski, Millhouse & Schenk-Strauss, 1984) allows real-time monitoring of both intensity and polarization of the primary beam. Monochromatic radiation was obtained from a Ge(111) double-crystal monochromator with 0·3–2·2 Å wavelength range, $\Delta E/E = 4\times10^{-4}$ energy resolution at 1 Å, and a harmonic suppression of $I_0(\lambda/3)/I_0(\lambda) < 10^{-3}$.

The majority of the measurements was carried out during dedicated shifts (3·7 GeV) of the DORIS II storage ring. Average runs lasted up to six hours with the ring current decreasing from 90 to 30 mA. Beam steering used the position monitors in beam port D where the diffractometer is located. An additional data set for Cu_2O was collected in parasitic mode (high-energy operation at 5·3 GeV) when fills last only about 60 min under considerably less-stable conditions (no beam steering). A high parasitic background from >80 keV photons is present, and the intensity is reduced on average by about 60% (ring current 40–20 mA). The latter measurements served to check the data reduction procedure and to assess the accuracy of data taken under less-favorable working conditions.

For all cases the wavelength was set close to 0·56 Å, and the beam was collimated to 1 mm diameter. For strong reflections (>20 000 counts s^{-1}), the intensity was reduced by insertion of appropriate filter combinations.

(*a*) *Preliminary work*

After optical centering of the crystal and refinement of the orientation matrix careful checks were made for:

(i) stability of crystal alignment and beam homogeneity by comparison of equivalent reflection intensities;

(ii) beam contamination by third- and fourth-order harmonics. Scanning of extinct reflections or of reflections with broken indices yields the remaining contribution of higher-order harmonics alone. The effect was then reduced to negligible importance by both slightly detuning the monochromator and adjusting the single-channel analyzer (SCA);

(iii) optimal detector aperture. Intensity profiles of equivalent reflections at medium scattering angle were measured at various aperture settings in order to obtain the full intensity record at lowest possible background;

(iv) optimal scan range. Although the small beam divergence yields sharp intensity profiles which are mainly determined by the mosaic spread of the crystal (typical FWHM 0·03° for Cu_2O and 0·02° for Al_2O_3), scans of increasing widths show long-ranging intensity tails which must be taken into account for valid background subtraction. Fig. 1 shows as an example reflection 220 of Cu_2O recorded with both synchrotron and Ag $K\alpha$ radiation. For correct numerical integration of the intensity profiles sufficiently small setting increments around the peak maximum are required. As already described by Nielsen *et al.* (1986), such profiles can be recorded most efficiently by using spread scans. Unfortunately, no such option was available for our experiment, so that considerable time was 'wasted' on background measurements due to the equidistant step scans. This point deserves attention in forthcoming work. Even

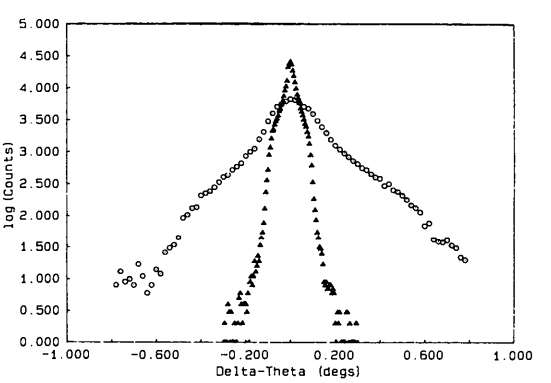

Fig. 1. Reflection 220 of Cu_2O recorded with both synchrotron radiation (circles) and Ag $K\alpha$ tube radiation (triangles), on logarithmic scale.

a pessimistic estimate shows that the data collection rate could be easily improved by a factor of two by reasonable tailoring of the step sizes.

(*b*) *Beam monitoring, filters and dead-time correction*

The preliminary work was completed by determination of the filter correction factors and the effective dead time of the counting chain (amplifier-discriminator, typically 4–8 μs). With the method of Chipman (1969), these parameters can be derived simultaneously from repeated measurements of reflections that require different filtering at the beginning and end of a fill. In the high energy shifts, the intensity drop of the primary beam is usually not large enough to make the method work satisfactorily. In this case additional filters have to be inserted to ensure a sufficiently wide variation of the primary intensity I_0.

Contrary to the considerations of Nielsen *et al.* (1986), the time structure of the non-continuous source caused no problems in our case. With 4×10^6 bunches s^{-1} (DORIS II, 4 bunch mode), the average bunch separation of 0·25 μs is much smaller than the dead time of the counting chains. With a limitation to a maximum count rate of 20 000 counts s^{-1} only negligible corrections are obtained using the above authors' equations (see also Arndt, 1978).

Beam monitoring and intensity normalization were then checked by measuring a strong reflection continuously during one or two complete fills. This measure provides a good test for the validity of the time-dependent corrections. Significant increase of the intensity with time indicates overload of the detector, *e.g.* due to insufficient filtering. In this case the monitor count rate was observed to decrease with decreasing ring current while the maximum peak count rate remained almost unaffected.

An apparent change of the reflection intensity with time can be attributed to a systematic error in the dead-time correction and the on-line normalization of the detector counts according to

$$N_{\rm corr} = N_c(1-t_mN_m)/N_m(1-t_cN_c)$$
$$= (N_c/N_m)[1-t(N_c+N_m)+t^2(N_cN_m+N_m^2)]. \quad (1)$$

N_c and N_m are the detector and monitor count rates recorded for the window settings of their respective single channel analyzers (SCA's), and $t_m \simeq t_c \simeq t$ are the associated dead times. However, N_c and N_m may not represent the true load of the detectors if they receive significant amounts of stray radiation of predominantly higher energy. This occurs only rarely during dedicated ring operation, but decrease of the normalized reflection intensity by a few per cent has been observed repeatedly during parasitic runs when DORIS II is operated at 5·3 GeV. Then, correct assessment of the reflection intensity would require in principle additional records of the SCA's integral mode outputs (for every scan step or at least before and after a scan) and/or beam shielding within the monochromator and around the detectors that guarantees complete absorption of all synchrotron light of undesired energy. This deserves consideration in future designs of diffraction stations.

According to (1) a simple empirical correction can be made by deriving an effective monitor dead time $t'_m > t_m$ from the intensity decrease of the check reflection and by applying t'_m in the course of data reduction. Fig. 2 shows, as an example, that using 16 μs effective dead time removes the intensity decrease completely, thus indicating a valid treatment of the problem.

(*c*) *Data collection*

Details of data collection are summarized in Table 2. A prescan was used to adjust the scan speed to the actual reflection intensity. The time per step was such that the counts at the peak maximum did not exceed 5000 per step (after insertion of filters). The allowed time range was 0·5–2 s for Cu_2O and 0·3–2 s for Al_2O_3, respectively.

Cu_2O. The orientation matrix was refined from the optimized angular settings of 16 reflections (511 and symmetry equivalents, $2\theta = 39{\cdot}85°$) yielding a_o = 4·2685 (5) Å. 511 was also used as check reflection and was remeasured every 30 min and at the beginning of each fill. The data collection comprised [$s = (\sin\theta)/\lambda$]:

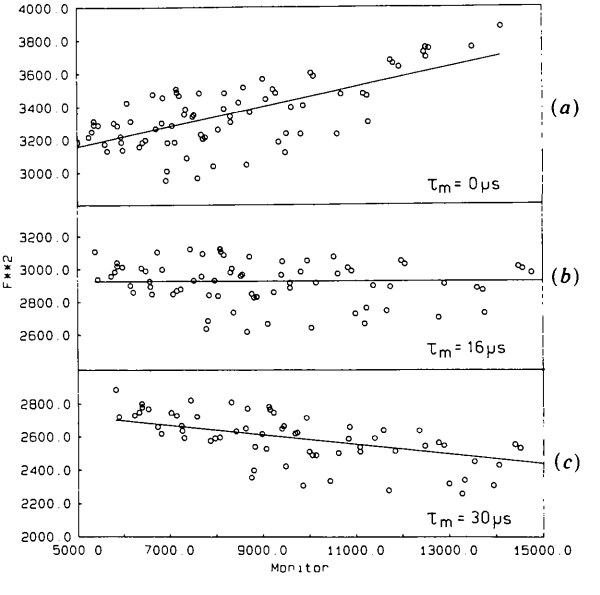

Fig. 2. Intensity of the Cu_2O check reflection 511 as a function of the monitor counts for (*a*) $t_m = 0$, (*b*) $t_m = 16$, and (*c*) $t_m = 30$ μs effective monitor dead time (counter dead time 8 μs). Note that monitor counts decrease during a fill.

Table 2. *Data collection and processing (CUL and CUH refer to dedicated and parasitic modes, respectively)*

Instrument	Five-circle diffractometer, HASYLAB		
Monochromator	Flat double crystal, Ge(111)		
Collimator	1 mm diameter		
Detector aperture	2×2 mm; 3×3 mm (CUH)		
Detector-sample distance	248 mm		
	Cuprite, Cu_2O	Corundum, Al_2O_3	
Sample	Natural, spherical	Synthetic, spherical	
Diameter	0·173(2) mm	0·200 mm	
Temperature	Ambient (295 K)		
	CUL	CUH	
Wavelength (Å)	0·5599 (1)	0·5616 (1)	0·5599 (1)
$(\sin\Theta/\lambda)_{max}$ (Å^{-1})	1·40	1·25	1·024
Scan mode	ω–2θ step scans		
Steps	121	121	91
Scan angle 2θ(°)	1·2	1·2	0·63
Scan speed (°min^{-1})	0·2–1·2	0·2–1·2	0·277–1·40
Check reflections	5,1,1		3,3,18 and 3,3,$\overline{18}$
Monitor interval	30 min and begin of a fill		
Number of reflections measured	342	324	1758
Number unique	133	134	259
Number unobserved	9 ($I<3\sigma$)	20 ($I<2\sigma$)	None ($I<3\sigma$)
$R_{int}(F)$		0·017	0·014
$R_{int}(I)$		0·028	0·032

(i) 125 reflections of all parities with $0<s\leq 1{\cdot}087$ Å^{-1}, $h\geq k\geq l\geq 0$, 120 unique;

(ii) 37 (*ooe*) 'oxygen' reflections with $1{\cdot}08<s\leq 1{\cdot}40$ Å^{-1}, $h\geq k\geq l\geq 0$, 34 unique;

(iii) 127 (*eeo*) 'forbidden' reflections with $0<s\leq 1{\cdot}055$ Å^{-1}, 23 unique. Including 53 check reflections, a data set of 342 reflections (hereafter referred to as CUL) was recorded within 64 h of which 35 h were effectively spent on the intensity scans. The scattering distribution of the check reflection is given by the relative e.s.d. $\sigma_{scatter}/I=0{\cdot}019$ equalling the mean relative e.s.d $\sigma[I(511)]/I(511)=0{\cdot}019$.

A second data set (CUH) was collected during high-energy operation (no beam steering, polarization 65–90%). With scan parameters identical to those of the previous measurements, 324 reflections were recorded: $\pm h\pm k\pm l$, $0<s\leq 0{\cdot}82$ Å^{-1}; $h\geq k\geq l\geq 0$, $0{\cdot}82<s\leq 1{\cdot}25$ Å^{-1}.

Al_2O_3. The orientation matrix was refined from 16 reflections with $41<2\Theta<64°$ yielding $a_o=4{\cdot}7570\,(5)$, $c_o=12{\cdot}9877\,(35)$ Å. Two check reflections 3,3,18 and 3,3,$\overline{18}$ were used similar to Cu_2O. Including 205 standard measurements, 1758 reflections $\pm h$, $\pm k$, l with $0<s<1{\cdot}024$ Å^{-1} were recorded in 68 h effective beam time. Since inspection of the integral intensities indicated insufficient filtering for the strong reflections (even with the maximum available filter combination), 176 of these with maximum peak count rate exceeding 20 000 counts s^{-1} were removed and remeasured in 6 h using an additional Al filter placed in front of the filter box.

No significant differences or scatter was observed for the two check reflections. Their internal agreement was $R(I)=0{\cdot}026$ which compares well with the mean relative e.s.d. $\sigma(I)/I_{check}=0{\cdot}027$.

Data reduction

Data reduction was carried out using the program *REDUCE* (Eichhorn, 1987), including some of the ideas of Blessing, Coppens & Becker (1974), adapted to synchrotron data.*

(*a*) *Integral intensities*

Normalization to monitor counts and allowance for beam polarization may introduce both random and systematic errors into the profile data. For each profile count C_i there are two additional counts from the beam monitors for the horizontally and vertically polarized components, C_H and C_V, respectively. Assuming proper dead-time correction, beam intensity I_i and polarization ratio Q_i can be defined as

$$I_i=C_{H,i}+C_{V,i},\qquad Q_i=(C_{H,i}-C_{V,i})/I_i. \quad (2)$$

The simplest approach would be to scale each profile point individually to its associated I_i and Q_i. However, this method has a serious disadvantage. Since C_V is usually less than 10% of C_H, and the counting time per step is determined (within preset limits) by the reflection intensity, the small C_V would introduce an unacceptably large counting error. The total error would then be dominated by the monitors rather than by the reflection profile.

A better approach uses $\langle C_H\rangle$ and $\langle C_V\rangle$ averaged over the N profile steps, provided that drift and fluctuations in the beam can be properly accounted for. This improves statistics by a factor of $N^{1/2}$, and since N is typically about 100, the error will be reduced to 10% of that obtained by the 'naïve' method.

Thus, the following calculations are performed in *REDUCE*:

(i) without significant drift in C_H and C_V averages are taken and

$$I_0=\langle C_H\rangle+\langle C_V\rangle,\qquad Q=(\langle C_H\rangle-\langle C_V\rangle)/I_0;$$

(ii) otherwise a least-squares line fitted to $C_{H,i}+C_{V,i}$ is used to correct both monitor and profile counts;

(iii) if there are significant fluctuations in the monitor counts ('bumps') the 'naïve' method, *i.e.* a point-per-point normalization is applied.

Since the contributions from both counting statistics and error propagation are taken into account, a profile with fluctuating monitor counts is

* Lists of structure factors for both Cu_2O and Al_2O_3 and multipole parameters for Al_2O_3 have been deposited with the British Library Document Supply Centre as Supplementary Publication No. SUP 52453 (15 pp.). Copies may be obtained through The Technical Editor, International Union of Crystallography, 5 Abbey Square, Chester CH1 2HU, England.

automatically given a larger e.s.d. than data collected under stable conditions.

(*b*) *Lp correction*

Integral intensities were determined using the Lehman–Larsen algorithm (Lehman & Larsen, 1974), and the Lp correction was applied in the usual way. For synchrotron radiation and vertical scattering geometry, the polarization factor is given by

$$P = 0{\cdot}5[(1+Q)+(1-Q)(1+\cos^2 2\theta)]. \quad (3)$$

The Lp correction is not a critical point in data reduction. Fig. 3 shows that for a medium scattering angle (35°) and complete neglect of the polarization correction even a change in polarization from 90 to 100% would affect the derived intensity by only 1·7%. Thus, errors in the assessment of the degree of polarization are less dramatic than might be expected. In agreement with Nielsen *et al.* (1986), Fig. 3 also shows that the choice of a short wavelength reduces the sensitivity of the measurements to the polarization.

(*c*) *Absorption and TDS correction*

Absorption corrections were computed using the factors A^* tabulated by Dwiggins (1975). For Cu_2O absorption factors A^* ranged from 4·07 to 5·34 (CUL) and 4·27 to 5·34 (CUH); for Al_2O_3 they do not vary over the data range.

The correction $(1+\alpha)$ for thermal diffuse scattering was evaluated with a modified version of the program *SXTDS*1 by Merisalo & Kurittu (1978). The elastic constants for the Cu_2O TDS correction were taken from Hallberg & Hanson (1970). The correction is nearly isotropic as pointed out by RS. The maximum corrections were 1·318 at 1·4 Å^{-1} (CUL) and 1·204 at 1·25 Å^{-1} (CUH). For Al_2O_3 elastic constants of Landoldt-Börnstein (1966) were used; the correction is almost negligible with a maximum value of 1·0053.

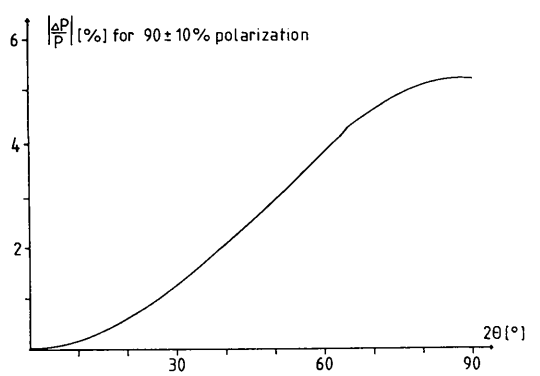

Fig. 3. Relative error $\Delta P/P$ in the polarization factor for a 10% change in the degree of polarization Q (defined in the text) as a function of the scattering angle 2θ.

(*d*) *Data averaging*

Weighted averages of symmetry-equivalent and multiply measured reflections were calculated in the usual way with e.s.d.'s being determined by both counting statistics and scatter.

Cu_2O. Averaging of the reduced CUH data yielded 134 unique reflections with internal consistency $R_{int}(F) = 0{\cdot}017$. 20 (*ooe*) and (*eeo*) reflections were considered unobserved ($\langle I\rangle < 3\sigma$).

The complete reduced and averaged data set CUL consisted of 133 unique reflections [22 (*eee*), 17 (*ooo*), 71 (*ooe*) and 23 (*eeo*)] of which 5 (*ooe*) and 4 (*eeo*) were considered unobserved ($\langle I\rangle < 2\sigma$). A conventional refinement showed that the intensities of the three strongest reflections, 111, 200 and 220, were calculated too large, probably due to insufficient filtering. Therefore, these reflections and seven other dubious reflections [5 (*ooe*), 2 (*eeo*)], possibly affected by *Umweganregung*, were excluded from all ensuing calculations, and the residual index dropped to $R(F) = 0{\cdot}022$. Considering the relatively large amount of weak and very weak reflections, this result signalled a data quality comparable to careful tube measurements.

A comparable data set (RS, $s_{max} = 1{\cdot}5$ Å^{-1}) was prepared from the 100 K literature data deposited by RS.

In order to estimate the agreement between the RS and CUL data (though taken from different crystals at largely differing temperatures) and to test a merged data set, the following procedure was carried out. [Adjusting the data to ambient temperature was necessary because there was no way of predicting correctly low-temperature structure amplitudes of the measured (*eeo*) reflections. Thus, the reverse procedure had to be discarded.]

(i) The RS data were conventionally refined, including isotropic extinction (as described below) to $R(F) = 0{\cdot}0103$ in agreement with RS.

(ii) With the linear temperature dependencies of the copper and oxygen U_{ij} as obtained from neutron diffraction experiments by Mullen & Fischer (1981), the atoms were allocated room-temperature values, and corresponding F_c(RT) and F_c(100 K) were calculated.

(iii) The observed RS data were individually scaled by $F_c(\mathrm{RT})/F_c(100\ \mathrm{K})$ yielding a set of F_{obs}(RT,RS).

(iv) In order to correct for possible errors in the allocated U_{ij} values and to scale the CUL data to the RS data, the F_{obs}(RT, RS) data were then fitted to the isotropic-extinction-corrected CUL data by minimizing

$$\{F_{obs}(\mathrm{CUL}) - KF_{obs}(\mathrm{RT,RS}) \times \exp[-B(h^2+k^2+l^2) - C(hk+hl+kl)]\}^2,$$

K being a scale factor, and B and C being adjustable

parameters which turned out not to differ significantly from zero. However, the corrections which were actually applied corresponded to $\Delta U = 72 \times 10^{-5}$ Å^2 for the strong and to $\Delta U = -75 \times 10^{-5}$ Å^2 for the oxygen reflections. Thus F_{obs}(RT,RS) received an additional correction according to these ΔU. The agreement factors obtained for each of the two reflection groups were $R(F) = 0{\cdot}0135$ and 0·040, respectively. The overall agreement for all reflections common to both data sets was 0·020.

Finally, a joint data set, JOIN, with $s < 1{\cdot}5$ Å^{-1} was prepared by weighted averaging of the common reflections. This final data set comprised 170 reflections of which altogether 18 (*ooe*) and 21 (*eeo*) were newly observed reflections and the weights of the averaged (*ooe*) reflections were increased considerably.

Al_2O_3. 1548 reflections were averaged to 259 unique reflections with an internal consistency $R_{int}(F) = 0{\cdot}014$ indicating good data quality. None of the reflections was considered as unobserved.

From the literature data deposited by LSF (set II, Ag $K\alpha$ data) a set of corresponding reflections ($s \leq 1{\cdot}024$ Å^{-1}) was prepared for comparable refinements.

Data analysis

(*a*) *Independent-atom-model (IAM) refinements*

The positional and thermal parameters reported by RS and LSF, respectively, were used as starting values for conventional independent-atom (IAM) structure refinements on $|F|$ with weights $w = [\sigma^2(F) + (PF)^2]^{-1}$. Scattering factors for neutral Al and O atoms were calculated from the Hartree–Fock (HF) wave functions given by Clementi & Roetti (1974). Neutral Cu-atom scattering factors were taken from *International Tables for X-ray Crystallography* (1974). Anomalous-dispersion corrections were taken from Cromer & Liberman (1971), and an isotropic extinction correction (Becker & Coppens, 1974) was included in all refinements. For both crystals type 1 and 2 models with Gaussian or Lorentzian distributions were tested. They all yielded practically identical results with marginal preference for a type 1 Lorentzian distribution. This type of correction was used in all ensuing refinements.

(*b*) *Multipole refinements*

Full data multipole refinements were carried out with the program *VALRAY* (Stewart, 1976; Stewart & Spackman, 1981). The total density in the asymmetric unit is assumed to be the sum of localized pseudoatom densities ρ_{at}. The density with respect to its nucleus of each pseudoatom p is given by

$$\rho_p(\mathbf{r}_p) = \mathrm{Pop}_p^{sph}\rho_p^{sph}(r_p) + \Delta\rho_p(\mathbf{r}_p) \qquad (4)$$

Table 3. *Details of the multipole refinements on* Cu_2O *and* Al_2O_3

Function minimized: $Q = \sum_h w_h[F_o(h) - kY(h)^{1/2}F_c(h)]^2$.
F_{obs} weights: $w_h = [\sigma^2(F) + (PF)^2]^{-1}$.
Deformation functions SEF of type $r^n \exp(-\alpha_l r)$, normalized to 1 electron for $l = 0$.

	l values	0	1	2	3	4
Cu	n	3		2		4
	$\alpha_{l,0}$	5·0				
Al	n	5	2	2	3	4
	$\alpha_{l,0}$	4·5				
O	n	3	2	2	3	4
	$\alpha_{l,0}$	4·5				

Constraints: Cu_2O: Pop(sph,Cu) : Pop(sph,O) = 29 : 8; Pop(0,Cu) = −0·5Pop(0,O)
Al_2O_3: Pop(sph,Al) : Pop(sph,O) = 13 : 8; Pop(0,Al) = −1·5 Pop(0,O).

$\alpha_{l,0}$ are the starting values for all multipole orders.

with

$$\Delta\rho_p(\mathbf{r}_p) = \sum_l \sum_{m=0}^{l} \left[\sum_i \mathrm{Pop}_p(l, m, i)\rho_p(l, r_p) \right] Y_{lm}^{\pm}(\theta, \Phi), \qquad (5)$$

r_p, θ and Φ are polar coordinates of $\mathbf{r}_p$, $Y_{lm}^{\pm}(\theta, \Phi)$ are Tesseral harmonics, and $\rho_p^{sph}(r_p)$ is the unperturbed spherical density of atom p, normalized to one electron. The index i in (5) indicates the option of using more than one radial deformation function per multipole order. The radial distribution functions $\rho_p(l, r_p)$ are chosen as single exponential functions (SEF's) of the type

$$\rho_p(l, r_p) = N_{n,l} r^n \exp(-\alpha_{p,l} r_p) \text{ with } n \geq l \qquad (6)$$

and

$$N_{n,l} = (1/4\pi)\alpha^{n+l+3}/(n+l+3)! \qquad (7)$$

Each pseudoatom is considered to be a rigid entity. Therefore, the thermal motion is taken to be the same for all multipole functions assigned to one atom. Each atom was assigned one monopole, and all allowed α_l were treated as variables. Monopolar populations Pop^{sph} were constrained to ensure neutrality. For Al_2O_3, correlation of the extinction with the deformation parameters, in particular with the α's, was obvious. Therefore, the extinction correction factor obtained from the all-data refinement was varied with proper damping throughout the multipole refinements. For Cu_2O the refined extinction corrections were negligible due to the correction on the basis of IAM. Crystallographic standard parameters, multipole populations, and α's were varied in alternating cycles. This procedure improves convergence of the rather flexible multipole model, but leads to underestimated standard deviations. However, since all refinements were carried out in the same way, the e.s.d.'s can be considered to indicate the significance of the variables achieved for the respective data sets. Details of the refinements are summarized in Table 3.

Table 4. Cu_2O *refinement results* ($U_{ij} \times 10^5 Å^2$) (*see text for details*)

		CULH	CULA	CUHH	RSH	RSA	JOIN
Cu	U_{11}	1917(6)	1908(6)	1975(7)	757(1)	757(1)	1900(4)
	U_{12}	−83(1)	−81(1)	−86(2)	−31(2)	−28(2)	−84(1)
	Q	−0·43(2)	−0·46(2)	−0·33(7)	−0·37(5)	−0·33(4)	−0·38(2)
	$\alpha(2)$	3·95(8)	3·89(6)	3·88(6)	3·67(23)	3·92(20)	4·20(20)
	H_1	0·23(5)	0·20(4)	0·61(14)	0·33(15)	0·37(20)	0·28(6)
	H_2	0·10(9)	0·18(7)	0·13(13)	0·18(3)	0·20(4)	0·20(11)
	$\alpha(4)$	7·4(4)	7·3(3)	7·3(4)	6·8(2)	6·4(2)	7·0(3)
O	U_{iso}	1879(7)	1891(7)	1958(17)	827(8)	828(8)	1880(7)
	Oct	−9·4(1·8)	−8·8(1·6)	0(3)	−8·8(8·0)	−2(3)	−9·4(1·9)
	$\alpha(3)$	2·46(8)	2·52(8)	4(32)	2·5(5)	3(1)	2·44(8)
CT		0·68(14)	0·72(14)	0·42(22)	0·54(4)	0·58(4)	0·56(11)
∇E_{zz}		135(6)	140(6)	104(22)	127(7)	144(7)	131(7)
P		0·02	0·02	0·02	0·0	0·0	0·02
R		0·0173	0·0168	0·0188	0·0065	0·0065	0·0106
wR		0·0296	0·0285	0·0523	0·0056	0·0056	0·0281
GOF		1·05	1·05	1·08	0·91	0·91	1·09
NO		123	123	111	129	129	170
NV		15	20	15	15	20	15

The temperature-factor expression is $\exp[-2\pi^2 \sum_i \sum_j U_{ij} h_i h_j a_i^* a_j^*]$.
CT = charge transfer in electrons from Cu towards O.
∇E_{zz} = electric field gradient ($V m^{-2} \times 10^{-20}$) along Cu–O at Cu site.
CULH = synchrotron data, dedicated operation, harmonic, $s_{max} = 1{\cdot}40$ Å^{-1}.
CULA = synchrotron data, dedicated operation, anharmonic, $s_{max} = 1{\cdot}40$ Å^{-1}.
CUHH = synchrotron data, parasitic operation, harmonic, $s_{max} = 1{\cdot}25$ Å^{-1}.
RSH = 100 K tube data as deposited by RS, harmonic, $s_{max} = 1{\cdot}50$ Å^{-1}.
RSA = 100 K tube data as deposited by RS, anharmonic, $s_{max} = 1{\cdot}50$ Å^{-1}.
JOIN = room temp. joint data (see text), harmonic, $s_{max} = 1{\cdot}50$ Å^{-1}.

All refinements were carried out in a straightforward way, systematic studies of the deformation model and/or weighting schemes were not attempted, since they are beyond the scope of this work. However, for both compounds we have also refined the deposited literature data of RS and LSF separately, using the same multipole models in order to avoid interpretation problems that might be caused by different modelling of the density (van der Wal, Vos & Kirfel, 1987). Thus, for both compounds the results may be biased by the models, refinement strategy and reflection weighting. However, since for each compound the refinement conditions were kept constant, differing results may be safely attributed to the data rather than to their handling.

Deformation properties

With the positional and thermal parameters from the multipole refinements, Fourier maps of interesting sections were calculated according to Stewart (1979). The dynamic deformation density is defined as

$$\Delta\rho_{dyn}(\mathbf{r}) = (2/V) \sum \Delta F(\mathbf{h}) \cos(2\pi \mathbf{h} \cdot \mathbf{r}) \quad (8)$$

with

$$\Delta F(\mathbf{h}) = [K|F_o(\mathbf{h})| - |F(\mathbf{h})_c^{IAM}|] \exp[i\Phi(\mathbf{h})_c^{mult}]. \quad (9)$$

The static deformation density is obtained directly from direct-space calculations according to

$$\Delta\rho_{stat}(\mathbf{r}) = \sum_{sym} \sum_p [\rho_p(\mathbf{r}-\mathbf{r}_p) - \rho(\mathbf{r}-\mathbf{r}_p)_p^{IAM}] \quad (10)$$

Table 5. *Structure factors of 'forbidden' (eeo) reflections of* Cu_2O, *after refinement CULH*

hkl	F_{obs}	F_{calc}	*hkl*	F_{obs}	F_{calc}
221	0·603 (3)	0·590	621	0·372 (4)	0·382
223	0·398 (8)	0·376	623	0·324 (14)	0·283
225	0·147 (37)	0·138	641	0·506 (6)	0·515
227	0·078 (39)	0·068	643	0·411 (15)	0·397
421	0·600 (5)	0·611	645	0·235 (19)	0·258
423	0·376 (16)	0·370	661	0·447 (7)	0·436
425	0·175 (25)	0·198	663	0·368 (12)	0·353
427	0·078 (44)	0·102	821	0·254 (18)	0·218
441	0·661 (5)	0·685	823	0·078 (44)	0·174
443	0·457 (8)	0·487	841	0·319 (14)	0·316
445	0·208 (64)	0·282			

Agreement index $R(F) = 0{\cdot}068$ (0·055 omitting 823).

where $\rho_p(\mathbf{r}-\mathbf{r}_p)$ is a pseudoatom density and $\rho(\mathbf{r}-\mathbf{r}_p)_p^{IAM}$ is the IAM density at site p.

Results and discussion

(*a*) *Refinement results*

Relevant refinement results are listed in Tables 4–6 and are discussed separately for Cu_2O and Al_2O_3.

Cu_2O. Allowed hexadecapolar deformations on the O atom turned out to be insignificant and were therefore omitted. All refinements converged readily to the values listed in Table 4. The results can be summarized briefly as follows.

(i) The anisotropy parameter U_{12}(Cu) is always negative indicating a preferred Cu vibration normal to [111], the Cu–O bond axis, as expected.

Table 6. Al_2O_3 *refinement results, fractional coordinates* $\times 10^5$, U_{ij} $Å^2 \times 10^5$

		IAMSY	MUSY	IAMLSF	MULSF
Al	z	35 220 (1)	35220 (1)	35218 (2)	35218 (1)
	U_{11}	236 (5)	242 (2)	257 (8)	259 (3)
	U_{33}	252 (6)	246 (3)	261 (10)	276 (5)
O	x	30631 (3)	30627 (2)	30617 (9)	30625 (5)
	U_{11}	265 (5)	265 (3)	305 (13)	292 (7)
	U_{22}	285 (2)	288 (3)	329 (16)	325 (9)
	U_{33}	313 (7)	310 (4)	333 (15)	334 (8)
	U_{23}	66 (3)	66 (2)	68 (12)	79 (7)
CT			1·17 (12)		2·12 (20)
P		0·0	0·0	0·0	0·0
R		0·0107	0·0078	0·0177	0·0128
wR		0·0141	0·0102	0·0172	0·0086
GOF		1·39	1·00	3·79	1·98
NO		258	258	258	258
NV		10	40	10	40

CT = charge transfer in electrons from Al towards O.
IAMSY = IAM refinement of synchrotron data.
MUSY = multipole refinement of synchrotron data.
IAMLSF = IAM refinement of corresponding LSF data.
MULSF = multipole refinement of corresponding LSF data.
All refinements with $s_{max} = 1{\cdot}024$ $Å^{-1}$. The temperature factor expression is as defined in Table 4.

(ii) The 'forbidden' (*eeo*) reflections are predominantly determined by U_{12}(Cu). This can be seen in Fig. 4 which compares F_{obs} with the F_c contributions from both the anisotropic vibration and the deformation functions for some (*eeo*) reflections after completion of refinement CULH. A more detailed analysis shows that the U_{12} contribution increases from about 70% for 221 to more than 85% for the high-order reflections. Thus, contrary to expectation the 'forbidden' reflections contain only little information about $\Delta\rho$(Cu). This explains why the RS data [without (*eeo*) reflections] refine successfully with respect to the Cu deformation. The Cu deformation parameters obtained from both CULH and RSH show remarkable agreement. This indicates good quality of the synchrotron data as well as successful separation of charge redistribution and thermal smearing for both cases. Thus, we conclude that the (*ooe*) reflections carry the main information. Measurement of the 'forbidden' (*eeo*) reflections is certainly helpful in fixing U_{12}(Cu) and the Cu deformation functions, but it is not decisive for a correct determination of these properties of Cu. In particular the quadrupolar deformation determining the electric-field gradient at the Cu site (see below) turned out to be a rather stable property.

(iii) The (*eeo*) reflections are, however, important for the determination of the oxygen deformation. Table 4 (refinements RSH and RSA) shows that lack of (*eeo*) reflections leaves the octapolar deformation on the O atom practically undefined in agreement with RS, whereas inclusion of them yields a significant indication of a weak polarization of electron density towards the Cu atoms in agreement with the theoretical maps.

(iv) The refined formal charge transfer from Cu towards O varies between 0·54 and 0·72 electrons and is on average 0·61 (9) electrons, the e.s.d. being derived from the scatter. This leads to a formal notation of $Cu_2^{+0{\cdot}6}O^{-1{\cdot}2}$ in agreement with chemical expectation.

(v) The preparation of the joint data set was an attempt to combine the best of the tube and the synchrotron data. The strong reflections were certainly measured with greater accuracy by RS while the weak reflections were much better determined in the synchrotron experiment. In spite of the basic problem of merging data of such different origin, the refinement results indicate a successful combination of the virtues of both data sets, and they show that tube data can be enhanced and improved by additional measurements using synchrotron radiation.

(vi) As one of the main results of this study this last point is emphasized in Fig. 5 which shows an F_{obs} *vs* F_c plot for all added (*eeo*) reflections after

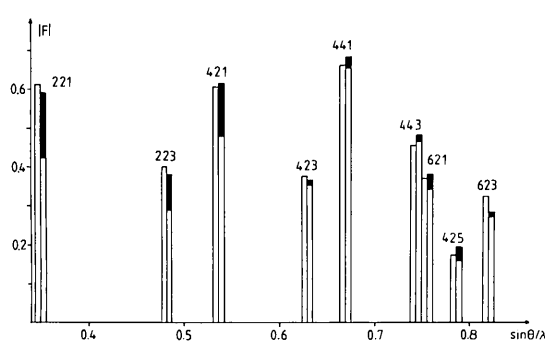

Fig. 4. Structure factors of the low-order 'forbidden' (*eeo*) reflections of Cu_2O. F_{obs} to the left, F_{calc} to the right, giving contributions from U_{12}(Cu) and $\Delta\rho$(Cu,O) (full black) separately.

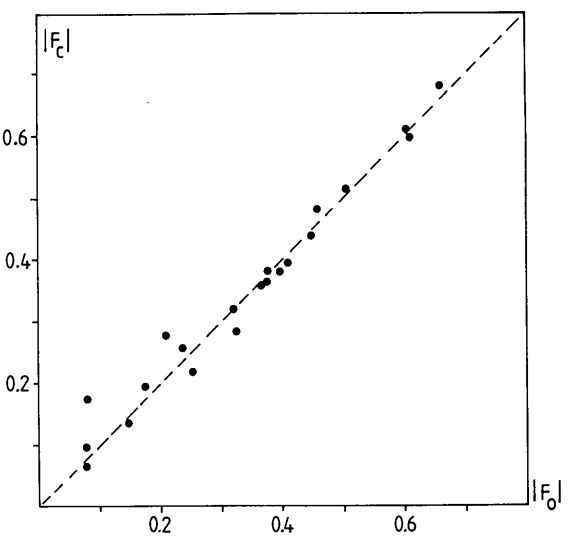

Fig. 5. Plot of F_{obs} *vs* F_{calc} for all 'forbidden' (*eeo*) reflections of Cu_2O after refinement CULH (Tables 4, 5).

refinement CULH. Table 5 contains the corresponding structure-factor list. The (*eeo*) agreement index of 0·068 (0·055 omitting 823) shows the quality of the very weak reflection intensities which contribute information that could never have been obtained by conventional X-ray tube experiments.

(vii) Table 4 also contains results of multipole refinements allowing for anharmonic vibration. The refined parameters are, however, not significantly different from those of the harmonic model. In particular, U_{12}(Cu) remained almost unaffected. An anharmonicity of the Cu vibration as discussed by RS cannot be supported by the present study.

(viii) Finally, Table 4 gives refinement results obtained with the CUH data collected during high-energy operation of DORIS II. These data are less complete and less accurate than CUL. Nevertheless, the refined parameters indicate the validity of the data reduction procedure and support our opinion that under less-favorable conditions reflection data can also be obtained from a synchrotron source with an accuracy sufficient at least for conventional structure analyses.

Al_2O_3. The conventional refinement [IAMSY (Table 6)] converged after a few cycles to a surprisingly low agreement index $R(F) = 0{\cdot}0107$ indicating only little anisotropic charge redistribution due to chemical bonding. Ten reflections had extinction correction factors $Y^{1/2} < 0{\cdot}9$; the most affected reflections were 300 0·64, 104 0·70 and 204 0·72. In full agreement with LSF the largest discrepancy occurred for reflection 006 as a consequence of the bond-induced charge transfer [$F_{obs}/F_c = 16{\cdot}20/12{\cdot}18$ compared to $F_{obs}(\mathrm{LSF})/F_c(\mathrm{LSF}) = 16{\cdot}79/12{\cdot}18$]. The parallel refinement, IAMLSF, yielded $R(F) = 0{\cdot}0177$ and GOF = 3·79.

The multipole refinements MUSY and MULSF converged readily to $R(F) = 0{\cdot}0078$ and 0·0128, respectively. Agreement of the refined positional parameters is very good while the vibrational parameters obtained from MULSF are larger by 10 (3)%. The formal charge transfer from Al towards O was different from the two refinements: MUSY 1·17(12) and MULSF 2·12 (20) electrons. The first figure is in fair agreement with the charges obtained by LSF as well as by Ngo Thong & Schwarzenbach (1979) for $AlPO_4$ and SiO_2.

The advantage that the use of synchrotron radiation can offer becomes evident when analyzing the observed and calculated structure factors of both data sets after completion of the multipole refinement.

Fig. 6 shows the internal agreement between the observed structure amplitudes, F^c_{obs}(Syn) and F^c_{obs}(LSF), and between the corresponding calculated quantities, F_{calc}(Syn) and F_{calc}(LSF), as functions of $|F|$. For both cases the agreement factor is defined as

$$R_{int} = \sum |F(\mathrm{Syn}) - F(\mathrm{LSF})| / \sum |F(\mathrm{Syn})|,$$

F^c_{obs} being corrected for extinction. Both $R_{int}(F)$ are nearly equal and close to 0·01 for $10 < |F| < 80$. $R_{int}(F_{obs})$ for $|F| > 80$ is larger due to extinction. The strongest reflection 300 is omitted in Fig. 6, the respective quantities are $F_{obs}(\mathrm{Syn}) = 138{\cdot}01$, $F_{calc}(\mathrm{Syn}) = 138{\cdot}19$, $F_{obs}(\mathrm{LSF}) = 131{\cdot}3$, $F_{calc}(\mathrm{LSF}) = 137{\cdot}69$, indicating an insufficient extinction correction in the case of the LSF data. For $1 < |F| < 5$ there are considerable discrepancies expressed by $R_{int}(F_{obs}) > 0{\cdot}13$ due to the obvious impossibility of obtaining weak reflection intensities more accurately with tube radiation. For this latter range of structure amplitudes $R_{int}(F_{calc})$ is close to 0·02, and less for all other reflections, showing the statistical equivalence of the

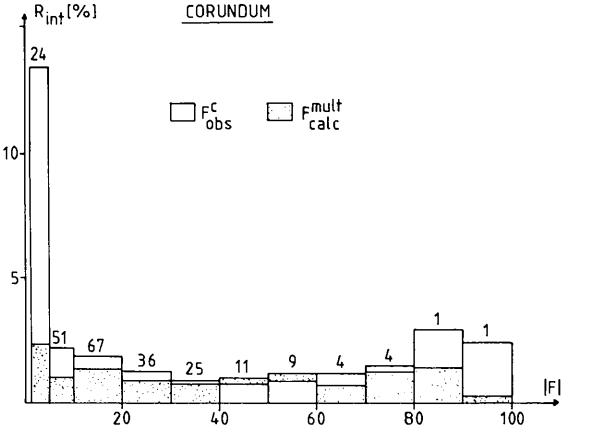

Fig. 6. Comparison of synchrotron and tube data for Al_2O_3. Internal agreement of corresponding extinction-corrected F^c_{obs} and F_{calc}, respectively. The number of contributors is given on top of each column.

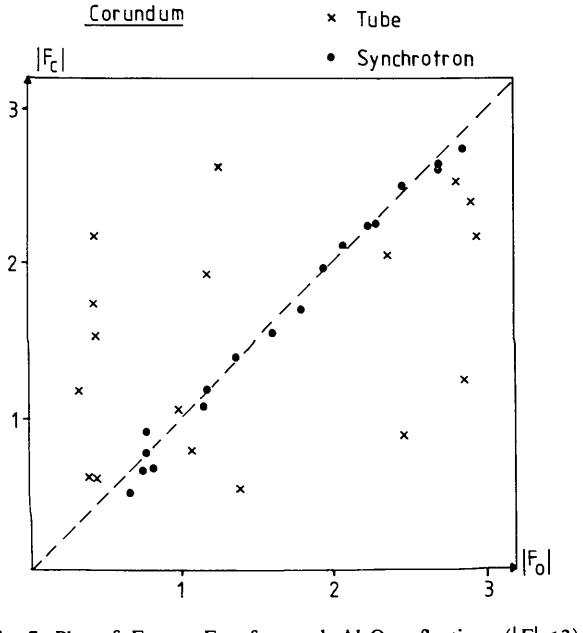

Fig. 7. Plot of F_{obs} *vs* F_{calc} for weak Al_2O_3 reflections ($|F| < 3$). Crosses: X-ray tube; circles: synchrotron data.

two refined models. Similar to Fig. 5 an F_{obs} *vs* F_{calc} comparison for reflections with $|F|<3$ and for both types of radiation is given in Fig. 7.

(*b*) *Deformation properties*

Cu_2O. As described by RS, omission of the 'forbidden' (*eeo*) and unobserved (*ooe*) reflections leads to a pseudo-translation effect (Cu atoms by $\frac{1}{2},\frac{1}{2},\frac{1}{2}$, O atoms by $\frac{1}{2},\frac{1}{2},0$) in the difference density maps, *i.e.* features around Cu and O are repeated at empty sites. On inclusion of calculated structure factors for the missing reflections the effect disappeared, and RS concluded that the combined contribution of those weak reflections is not negligible. The dynamic deformation density obtained after refinement JOIN (Fig. 8*a*) shows this to be true, no pseudo-translation effects are detectable.

All features of the corresponding residual density (Fig. 8*b*) are smaller than 0·15 eÅ^{-3} indicating that the observations were well modelled and scaled.

The main result of Fig. 8(*a*) is a significant charge depletion at the Cu site. This trough is elongated along the Cu–O bond and accompanied by symmetric charge accumulations off the bond in the [001] direction. The same feature is reproduced in the very similar static deformation density distributions resulting from both CULH and RSH, respectively (Figs. 8*c*, *d*). These maps show the model deformation density after deconvolution of thermal smearing. In keeping with the similar refinement results these maps are also very similar. This applies as well to the corresponding maps obtained after the anharmonic refinements CULA and RSA which are omitted since they reveal the same patterns. The prominent features of Figs. 8(*d*), (*e*) are a 'cross' of charge depletion parallel to [111] together with a second 'cross' of charge accumulation parallel to [001]. This picture becomes clearer upon omission of the monopolar deformation functions as shown in Figs. 8(*e*), (*f*). Exactly those characteristics were obtained from both linearized augmented plane-wave (LAPW) band-structure calculations by Marksteiner, Blaha & Schwarz (1986) and cluster calculations by Nagel (1985). The main difference between the theoretical maps and Figs. 8(*e*), (*f*) is found in the positive lobes. The former show smaller lobes of equal heights while the experimental densities reveal a preferred charge accumulation along [001]. This skewed pattern was obtained by RS and is reproduced by the completely independent synchrotron data. Consequently, it seems very likely that this is not an artifact, but implies some interaction in the crystal which is not taken into account by the quantum-mechanical calculations.

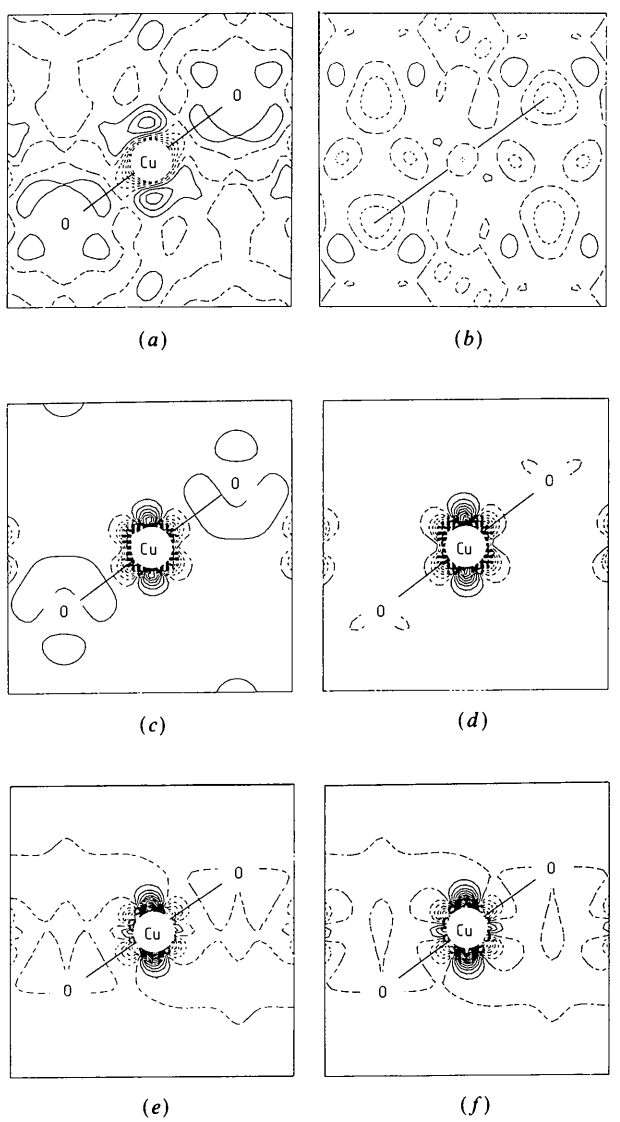

Fig. 8. Electron-density maps for Cu_2O in the plane (110). Horizontal axis: [110], vertical axis: [001]. O–Cu–O bonds along [111] are indicated. (*a*) Dynamic deformation density $\Delta\rho$ from refinement JOIN; (*b*) corresponding residual density, $s_{max}=0{\cdot}85$ Å^{-1}; (*c*),(*d*) static model deformation densities from CULH and RSH, respectively. Monopoles have been included. (*e*), (*f*) as (*c*) and (*d*), monopoles omitted. Contours at 0·05 eÅ^{-3} [0·1 for (*a*)], negative broken, positive full lines.

Al_2O_3. Figs. 9(*a*)-(*d*) show the static model deformation density distributions resulting from the independent multipole refinements MUSY and MULSF, respectively. The plane (010) of Figs. 9(*a*), (*b*) contains the Al atom in the center and the O atom at $x,0,\frac{1}{4}$ on a diad axis normal to [001]. The symmetry-equivalent O atom at $z=\frac{5}{12}$ is 0·12 Å out of the plane. The long bond (1·972 Å) points towards the face shared by adjacent oxygen octahedra, the short bond (1·855 Å) towards the unshared face. Both faces can be seen in Figs. 9(*c*), (*d*), showing the plane (001) which contains the O-atom layer at $z=\frac{1}{4}$. The *c* axis in the middle of the map runs through the center of the shared face. Thus, the two planes are identical to those published by LSF.

The deformation models obtained from the LSF and synchrotron data possess common features, but also show some disturbing differences which are probably caused by extinction problems. Common to both models is the charge migration from Al towards O, the polarization of the latter towards Al, especially on the long bond, and the appearance of an oxygen deformation outside the shared face (Figs. 9*c*, *d*). By combination of the information of both planes, the deformation of the oxygen valence shell takes the form of an sp^3 hybrid. While the symmetry-related charge accumulations on the long bonds are at most 0·15 eÅ^{-3} and clearly resolved in the MUSY map, they are about twice as large and smeared out to a banana shape in the MULSF map. This latter finding agrees well with the maps published by LSF and is similar to the results of Tsirelson, Antipin, Gerr, Ozerov & Struchkov (1985). This smeared deformation density appears in Fig. 9(*d*) as a third density lobe directed towards the center of the shared face, where the deformation density almost vanishes. The lack of such lobes in Fig. 9(*c*) is thus due to the resolved density lobes in Fig. 9(*a*) rather than to conflicting density models.

A further difference is found for the Al atom. The quadrupolar deformations possess opposite sign and are developed differently for the two data sets.

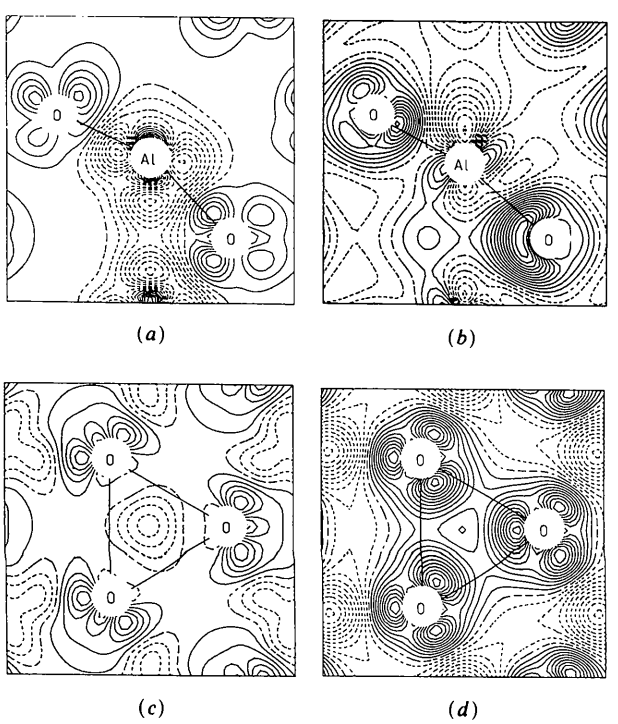

Fig. 9. Static model deformation density maps for Al_2O_3. (*a*), (*b*) Plane (010) through Al in (0, 0, *z*) and O in (x, 0, $\frac{1}{4}$); (*c*), (*d*) plane (001) through oxygen layer at $z=\frac{1}{4}$. (*a*), (*c*) Synchrotron data (MUSY); (*b*), (*d*) X-ray tube data (MULSF). Monopoles included; contours at 0·025 eÅ^{-3}, negative broken, positive full lines.

In order to check whether the observed differences are artifacts introduced by the model, conventional difference density maps were calculated for both data sets. These maps are omitted because they show essentially the same features as Fig. 9 so that correct modelling of the information contained in the respective data sets can be inferred. Hence, the differences must be attributed to the data and their extinction corrections, not to their refinements.

(*c*) *Electric field gradient*

Cu_2O. The electric field gradient (EFG) tensor at the Cu site is characterized by one component, ∇E_{zz} (z along [111]). From NQR measurements by Krueger & Meyer-Berkhout (1952) one of the largest known field gradients, $|\nabla E_{zz}| = 1{\cdot}34\times10^{22}$ V m^{-2} is obtained (RS). According to an ionic point-charge model (Hafner & Nagel, 1983) the sign of ∇E_{zz} is positive, whereas the cluster calculation by Nagel (1985) favors the opposite. The EFG results reported by RS are very model dependent with both negative and positive signs, their numerical values were disappointingly different from the NQR result.

Values for the EFG were determined by direct-space calculations according to Stewart (1979) and are included in Table 4. All refinements produced EFG's with positive sign and unexpectedly good numerical agreement with the NQR value of $1{\cdot}34\times10^{22}$ V m^{-2}. Even the EFG from the less-accurate CUH data is in the vicinity of this figure. The true relative e.s.d. was estimated to be about 60% by performing an additional dummy refinement cycle in which simultaneous variation of all model parameters was allowed. In spite of this large uncertainty it is found that the X-ray data do indeed contain information about the EFG at the Cu site.

Al_2O_3. The electric field gradients at both the Al and the O site are known from NQR measurements. Due to the site symmetry 3, the EFG at the oxygen position can be described by three figures, *i.e.* the largest eigenvalue ∇E_{zz}(O), the angle α subtended by the corresponding principal axis z and c_o, and the asymmetry parameter

$$\eta = (\nabla E_{xx} - \nabla E_{yy})/\nabla E_{zz}.$$

From the NQR results LSF calculated these figures as $\nabla E_{33}(\mathrm{Al}) = -6{\cdot}55\times10^{20}$ V m^{-2}, $\nabla E_{zz}(\mathrm{O}) = +3{\cdot}49\times10^{21}$ V m^{-2}, $\alpha = 45{\cdot}85°$ and $\eta = 0{\cdot}517$.

The corresponding values ($\times10^{-20}$ V m^{-2}) obtained from direct-space calculations for the models MUSY and MULSF (the latter in parentheses) are: $\nabla E_{33}(\mathrm{Al}) = -27$ (+24), $\nabla E_{zz}(\mathrm{O}) = -12{\cdot}5$ (+4), $\alpha = 50{\cdot}2°$ (53·4°) and $\eta = 0{\cdot}67$ (0·31). For ∇E_{33}(Al) both moduli are too large, but model MUSY exhibits the correct sign, whereas model MULSF gives the wrong sign similar to results obtained by LSF using an anisotropic extinction correction. For the O atom

(with the larger EFG) the situation is reversed: both moduli are too small, and now MULSF gives the correct sign. Common to both data sets is the correct determination of shape and orientation of the EFG tensor. Therefore, the EFG results are inconclusive. Without theoretical calculations there is hardly a basis to extract more information or to discriminate between the two refined models.

Summary and concluding remarks

This work was intended as a feasibility study in order to assess the accuracy of single-crystal reflection intensities measured at a synchrotron source, given the normal beam time allowance of ≤ 7 d. In order to permit a rigorous cross checking against existing tube data, Cu_2O and Al_2O_3 were chosen due to the availability of high-quality electron-density analyses, and the data were collected at the same wavelengths as the careful and time-consuming tube experiments. Emphasis was put primarily on the experiment and the ensuing data reduction procedure rather than on systematic and thorough electron-density studies with their inherent problems. The deformation density properties of both compounds were evaluated in a straightforward manner and yielded in general satisfactory agreement with the reference results. Differences in details are mainly due to the data treatment and in part to the refinement models. The judgement about the electron-density results is thus left to the reader, while the following more general conclusions concerning the use of synchrotron radiation can be drawn from the present results.

(i) The specific properties of synchrotron radiation cause no serious problems in single-crystal diffractometry. All relevant results indicate that in spite of the relatively fast data collection complete sets of structure amplitudes can be derived whose quality compares well with careful tube measurements, provided that there are stable beam conditions, and that proper attention is given to the performance of the experiment and to the data reduction. With respect to experimental strategy and data evaluation one can therefore be confident about the general feasibility of accurate structure analyses using synchrotron radiation. This result is of interest whenever crystals are to be studied at a specific wavelength, or when a short wavelength is deliberately chosen in order to reduce absorption, extinction and polarization effects.

(ii) Compared to tube measurements nothing is gained in the measurement of strong or medium intensity reflections, since for them the signal/noise ratio does not profit from the small beam divergence. Those reflections can be measured more conveniently and at much lower costs in the home laboratory. For synchrotron radiation, it should also be noted that any filtering of primary-beam intensity means giving away valuable beam time, and simultaneously introducing unnecessary errors into the data reduction. These arguments do not, however, hold in the case of: (*a*) selected measurements of strong reflections at various wavelengths in order to improve the data by experimental assessment of extinction effects; (*b*) new technical developments like faster counters which may eventually lead to considerable time savings in collection of stronger reflections.

(iii) Improvement of data can also be achieved by increasing the reliability of weak reflections. For these, Figs. 5 and 7 give one clear answer to the question when synchrotron radiation may be used most profitably in structure analyses. Since for synchrotron radiation there are virtually no 'unobserveds', and since the data carry similar uncertainties over a wide intensity range, the keyword is measurement of intensities which - in the home laboratory - are unobservable or close to unobservable because of large statistical errors. More accurately measured weak reflections will not only decrease the statistical noise in the refinements and Fourier maps, but will also alter the weighting scheme in favor of the high-order reflections (giving results closer to a high-order refinement). A data set comprising reflections with similar relative e.s.d.'s will provide an increased effective resolution and an improved determination of the crystallographic standard parameters. This is of special importance for electron-density analyses which require unbiased promolecule parameters for a successful separation of bonding effects. Since the collection of weak reflections is possible at a synchrotron-radiation source, such measurements are first-class candidates for a sensible single-crystal X-ray diffraction experiment. With respect to accurate crystal structure analysis we therefore conclude that enhancement of conventionally collected data by synchrotron measurements of selected reflections provides a very economical and promising method for future work.

The financial support for this work, granted by the Bundesminister für Forschung und Technologie is gratefully acknowledged. We are also indebted to D. Schwarzenbach for constructive discussions and to J. Sandoz et fils, SA, CH-1482 Cugy, Switzerland, for the Al_2O_3 samples.

References

ARNDT, U. W. (1978). *J. Phys. E*, **11**, 671-673.
BACHMANN, F., KOHLER, H., SCHULZ, H. & WEBER, H. P. (1985). *Acta Cryst.* A**41**, 35-40.
BECKER, P. J. & COPPENS, P. (1974). *Acta Cryst.* A**30**, 129-147, 148-153.
BLESSING, R. H., COPPENS, P. & BECKER, P. J. (1974). *J. Appl. Cryst.* **7**, 488-492.
CHIPMAN, D. R. (1969). *Acta Cryst.* A**25**, 209-214.
CLEMENTI, E. & ROETTI, C. (1974). *Atomic Data and Nuclear Data Tables*, Vol. 14, No. 3-4. New York: Academic Press.
CROMER, D. T. & LIBERMAN, D. A. (1971). *J. Chem. Phys.* **53**, 1891-1898.

DWIGGINS, C. W. (1975). *Acta Cryst.* A31, 395-396.
EICHHORN, K. (1987). *REDUCE. Program for Data Reduction of Step-Scan Measured Reflection Profiles for both Neutrons and X-rays.* DESY/HASYLAB, Hamburg, Federal Republic of Germany. Unpublished.
HAFNER, S. & NAGEL, S. (1983). *Phys. Chem. Miner.* 9, 19-22.
HALLBERG, J. & HANSON, R. C. (1970). *Phys. Status Solidi*, 42, 305-310.
International Tables for X-ray Crystallography (1974). Vol. IV. Birmingham: Kynoch Press. (Present distributor Kluwer Academic Publishers, Dordrecht.)
KOELLING, D. D. & ARBMAN, G. O. (1975). *J. Phys. F*, 5, 2041.
KRUEGER, H. & MEYER-BERKHOUT, K. (1952). *Z. Phys.* 132, 171-178.
KUPCIK, V., WENDSCHUH-JOSTIES, M., WOLF, A. & WULF, R. (1986). *Nucl. Instrum. Methods*, A246, 624-626.
KURKI-SUONIO, K. (1977). *Isr. J. Chem.* 16, 115-123.
LANDOLDT-BÖRNSTEIN (1966). Edited by K.-H. HELLWEGE. Neue Serie III-1, p. 13. Berlin: Springer Verlag.
LEHMANN, M. S. & LARSEN, F. K. (1974). *Acta Cryst.* A30, 305-310.
LEWIS, J., SCHWARZENBACH, D. & FLACK, H. D. (1982). *Acta Cryst.* A38, 733-739.
MARKSTEINER, P., BLAHA, P. & SCHWARZ, K. (1986). *Z. Phys.* B64, 119-127.
MERISALO, M. & KURITTU, J. (1978). *J. Appl. Cryst.* 11, 179-183.
MULLEN, D. & FISCHER, K. (1981). *Z. Kristallogr.* 156, 85-86.
NAGEL, S. (1985). *J. Chem. Phys. Solids*, 46, 743-756.
NGO THONG & SCHWARZENBACH, D. (1979). *Acta Cryst.* A35, 658-664.
NIELSEN, F. S., LEE, P. & COPPENS, P. (1986). *Acta Cryst.* B42, 359-364.
RESTORI, R. & SCHWARZENBACH, D. (1986). *Acta Cryst.* B42, 201-208.
SMEND, F., SCHAUPP, D., CZERWINSKI, H., MILLHOUSE, A. H. & SCHENK-STRAUSS, H. (1984). DESY Internal Report No. SR-84-003. DESY/HASYLAB, Hamburg, Federal Republic of Germany.
STEWART, R. F. (1976). *Acta Cryst.* A32, 565-574.
STEWART, R. F. (1979). *Chem. Phys. Lett.* 65, 335-342.
STEWART, R. F. & SPACKMAN, M. A. (1981). *VALRAY* Users Manual. Preliminary Draft. Department of Chemistry, Carnegie-Mellon Univ., Pittsburgh, PA 15213, USA.
TSIRELSON, V. G., ANTIPIN, M. YU., GERR, R. G., OZEROV, R. P. & STRUCHKOV, YU. T. (1985). *Phys. Status Solidi A*, 87, 425-433.
WAL, R. J. VAN DER, VOS, A. & KIRFEL, A. (1987). *Acta Cryst.* B43, 132-143.
WENDSCHUH-JOSTIES, M. & WULF, R. (1989). *J. Appl. Cryst.* 22, 382-383.

Acta Cryst. (1990). A46, 284-297

A Multisolution Method of Phase Determination by Combined Maximization of Entropy and Likelihood. I. Theory, Algorithms and Strategy

BY G. BRICOGNE

LURE, Université Paris-Sud, 91405 *Orsay, France*

AND C. J. GILMORE

Department of Chemistry, University of Glasgow, Glasgow G12 8QQ, Scotland

(*Received* 8 *August* 1989; *accepted* 15 *November* 1989)

Abstract

A new multisolution method for direct phase determination [Bricogne (1984). *Acta Cryst.* A40, 410-445] has been implemented and tested on small crystal structures. It consists of an organized search for those combinations of phases associated with a 'basis set' of reflexions which have *maximum likelihood, i.e.* which lead to the assignment of the highest conditional probability to the observed moduli belonging to reflexions outside the basis set. Phase choices are made sequentially, progressively enlarging the basis set, and the book-keeping involves a 'multisolution tree' which summarizes the parentage relations between them. The conditional probability distributions (c.p.d.'s) of structure factors used in evaluating the likelihood are derived from joint distributions obtained by the saddlepoint method. The latter involves distributions of atoms which have the *maximum entropy* compatible with all phase choices made, and hence are different for each node of the multisolution tree. These distributions q^{ME} are constructed numerically by exponentially modelling, coupled with a very robust plane search which often simplifies to a line search. C.p.d.'s of small numbers of structure factors not in the basis set are readily calculated from q^{ME}, with correct representation of their multimodality. A further 'diagonal' approximation of these c.p.d.'s allows the log-likelihood to be written as a sum of contributions from individual non-basis reflexions. The phasing process is initiated by specifying the origin-fixing and enantiomorph-defining phases, and forming the corresponding q^{ME}. It progresses by roughly locating the maxima of the c.p.d.'s of additional structure factors by a magic-integer technique, updating q^{ME} separately for each such maximum, and evaluating their respective likelihoods. The most likely phase sets are further refined

0108-7673/90/040284-14$03.00